Astron. Astrophys. 324, 1123–1134 (1997)

ASTRONOMY AND ASTROPHYSICS

The chemical evolution of planetary nebulae

R. Bachiller[1], **T. Forveille**[2], **P.J. Huggins**[3], **and P. Cox**[4,5]

[1] Observatorio Astronómico Nacional (IGN), Apartado 1143, E-28800 Alcalá de Henares, Spain
[2] Observatoire de Grenoble, B. P. 53X, F-38041 Grenoble Cedex, France
[3] Physics Department, New York University, 4 Washington Place, New York NY 10003, USA
[4] Institut d'Astrophysique Spatiale, Bât. 121, Université de Paris XI, F-91405 Orsay Cedex, France
[5] Institut d'Astrophysique de Paris, 92b bd. Arago, F-75014 Paris, France

Received 4 November 1996 / Accepted 19 February 1997

Abstract. We report millimeter line observations of CO, ^{13}CO, SiO, SiC_2, CN, HCN, HNC, HCO^+, CS, and HC_3N to study the chemistry in planetary nebulae (PNe) with massive envelopes of molecular gas. The sample observed consists of representative objects at different stages of development in order to investigate evolutionary effects: the proto-PNe CRL 2688 and CRL 618, the young PN NGC 7027, and the evolved PNe NGC 6720 (the Ring), M4-9, NGC 6781, and NGC 7293 (the Helix).

The observations confirm that the chemical composition of the molecular gas in PNe is radically different from that in interstellar clouds and the circumstellar envelopes of Asymptotic Giant Branch (AGB) stars. There are also clear trends in the chemical evolution of the envelopes. As a star evolves beyond the AGB, through the proto-PN and PN phases, the abundances of SiO, SiC_2, CS, and HC_3N decrease, and they are not detected in the PNe, while the abundances of CN, HNC, and HCO^+ increase dramatically. Once a PN has formed, the observed abundances in the molecular clumps of the envelope remain relatively constant, although HNC is anomalously underabundant in NGC 7027. In the evolved PNe, CN is about an order of magnitude more abundant than HCN, HNC, and HCO^+, and the average abundance ratios are CN/HCN = 9, HNC/HCN = 0.5, and HCO^+/HCN = 0.5. These ratios are, respectively, one, two, and three orders of magnitude higher than in the prototypical AGB envelope IRC+10216. The $^{12}C/^{13}C$ ratios are $\approx$10–25, within the large range found in AGB envelopes. The chemical evolution of the envelopes likely occurs through the development of photon-dominated regions produced by the ultraviolet radiation field of the central star.

The observations also provide important information on the physical conditions in the molecular gas. Multi-line observations of CN, CO, and HCO^+ show that the clumps which form the envelopes of the evolved PNe maintain remarkably high gas densities ($\sim$ few $\times 10^5$ cm^{-3}) and low temperatures ($\sim$25 K). These values are consistent with the idea that the clumps are in rough pressure equilibrium with the more diffuse, ionized gas and can last for a significant part of the nebular lifetime, providing the environment needed for the survival of the molecules. Thus the clumping of the gas in these PNe is an essential aspect of both their physical and chemical evolution.

Key words: planetary nebulae – stars: mass-loss – radio lines: stars

Send offprint requests to: R. Bachiller

1. Introduction

It is now well established that many planetary nebulae (PNe) are surrounded by massive envelopes of relatively cold molecular gas (Huggins & Healy 1989, Huggins et al. 1996). The molecular envelopes form highly fragmented, spheroidal shells or rings around the ionized nebulae, and their structure has been well documented by mapping the millimeter emission lines of CO and by infrared imaging of H_2 (Bachiller et al. 1989ab, 1993; Forveille & Huggins 1991; Cox et al. 1991; Sahai et al. 1991; Kastner et al. 1996).

The chemical composition of these PN envelopes is expected to be quite different from that in interstellar clouds or the circumstellar envelopes of AGB stars, because of the extreme physical conditions. The gas in PNe is exposed to very strong ultraviolet radiation fields from the evolving central stars, and probably to violent shocks generated by fast stellar winds. The envelopes thus provide unique environments for the study of chemistry under these extreme conditions, and the molecular abundances should provide useful diagnostics of processes which play important roles in the evolution of the nebulae.

In spite of the intrinsic interest of the chemistry in PNe, observational studies of the chemical composition of the molecular gas have been largely confined to the massive envelope of NGC 7027 because of the weakness of the lines in other envelopes. In addition to CO, NGC 7027 has been detected in lines of HCN (Olofsson et al. 1982), CN (Thronson & Bally 1986), C_3H_2 (Cox et al. 1988), HCO^+ (Deguchi et al. 1990), N_2H^+ (Cox et

al. 1993), and CO^+ (Latter et al. 1993), and in a forthcoming paper, we present a detailed study of the chemistry of the envelope (Cox et al. 1997, in preparation). In other PNe, HCN, HNC, and HCO^+ have been detected in NGC 2346 by Bachiller et al. (1989b); these molecules together with relatively strong emission from CN have been detected in NGC 6072 and IC 4406 by Cox et al. (1992); and similar results have been obtained in M1-16 by Sahai et al. (1994). The observations of these few PNe indicate that the molecular abundances in PNe are indeed unusual, and the objective of the current paper is to provide a more extensive study of the chemistry.

The observations reported here include a comprehensive search for line emission of nine molecular species in a sample of seven prototypical objects representing different evolutionary stages: the proto-PNe CRL 2688 and CRL 618, the young PN NGC 7027, and the evolved PNe NGC 6720 (the Ring), M4-9, NGC 6781, and NGC 7293 (the Helix). The observations also include multi-line observations to constrain the excitation and the physical conditions in the gas. The results of the observations substantially improve the available data on the chemistry in PN envelopes and provide the basis for a systematic study of the changes in the chemistry of the envelopes along an evolutionary sequence.

2. Observations and results

Most of the observations were carried out with the IRAM 30-m telescope at Pico Veleta (near Granada, Spain) in June 1991. The telescope was equipped with three SIS receivers operating in the λ 1, 2, and 3 mm bands, which provided system temperatures at the zenith of 1500, 600, and 400 K, respectively. The spectrometers were two filterbanks of 512×1 MHz channels, and one of 256×100 kHz which was used to resolve the narrower spectral lines. The antenna half-power beamwidth and the main beam efficiency were $12''$ and 0.45 at 220 GHz, $18''$ and 0.55 at 140 GHz, and $24''$ and 0.65 at 110 GHz. Pointing was checked every hour by observing nearby planets or continuum sources, and was found to be accurate within $3''$. All observations were made in position switching mode, and linear baselines were subtracted from the spectra.

Additional observations at shorter wavelengths in the λ 0.8 mm band and the 1 mm band were carried out with the CSO 10-m telescope at Mauna Kea (Hawaii, USA). SIS receivers operating in these two bands provided typical system temperatures at the zenith of 800–900 K. The spectrometers were an AOS of 1024×0.49 MHz channels, and one of 1024×49 kHz which was used to resolve the narrower spectral lines. The antenna half-power beamwidth and the main beam efficiency were $27''$ and 0.72 at 270 GHz, and $22''$ and 0.65 at 345 GHz. Pointing was checked by observing nearby planets or standard sources, and is estimated to be accurate within $5''$. The observations were made in position switching mode, and low degree polynomial baselines were subtracted from the spectra. The intensities of all the observations reported in this paper are given in units of main beam brightness temperature.

The coordinates of the PNe and the offset positions observed are given in Table 1, together with other relevant information. CRL 2688, CRL 618, and NGC 7027 were observed at the center position, but the more evolved, spatially extended PNe were observed at offsets selected from previous CO mapping. The CO line parameters at the observed positions are also are given in Table 1. The line widths are generally narrower for the more extended, evolved PNe because their shells are more completely resolved by the telescope beam.

Table 2 lists the molecular transitions and the observed line strengths or upper limits, in the form of velocity integrated line intensities. As a check on the intensities we remeasured some of the lines during two other observing runs with the 30-m telescope, with consistent results. Our measurements of the CO lines in CRL 2688, CRL 618, and NGC 7027 are also in agreement with most previous observations with the same telescope (e.g., Mauersberger et al. 1989; Bachiller et al. 1988; Cernicharo et al. 1989; Truong-Bach et al. 1990). We believe that the intensities reported here are accurate to better than 20%.

Fig. 1 shows the J=2−1 spectra of CO and ^{13}CO, and the J=1−0 spectra of HCN, HNC, and HCO^+ which were detected in all the objects in the sample. The ^{12}CO and ^{13}CO spectra of M4-9 and NGC 6781 are slightly contaminated by emission from molecular clouds along the line of sight, at velocities around 8.5 and 6 km s^{-1}, respectively. Fortunately, the contaminated regions are sufficiently offset from the nebular velocities that they do not significantly affect the measurement of the nebular lines and they have been blanked out in Fig. 1. Figs. 2–4 show the CN spectra in the N=1−0 and N=2−1 transitions which were detected in all the objects, and in the N=3−2 transition which was observed in four; Fig. 4 also includes CN N=3−2 observations of the two southern PNe NGC 6072 and IC 4406 which were previously observed in CN only in the N=1−0 line by Cox et al. (1992). Details of the complex CN spectra are discussed below (Sect. 3). HC_3N, SiO, CS, and C_3H_2 were detected only in CRL 2688 and CRL 618 and upper limits are obtained for the other PNe. Previous molecular line observations of CRL 2688 and CRL 618 have been reported by Bujarrabal et al. (1988) and Cernicharo et al. (1989).

3. Line opacities, excitation, and physical conditions in the molecular gas

We first discuss the observations of the molecular species for which we have measurements of more than one transition, i.e., CN, CO and HCO^+. These multi-line observations provide information on the excitation and opacity of the molecular lines which are important considerations for estimating abundances from the line intensities. The excitation also yields constraints on the physical conditions in the molecular gas.

3.1. CN profiles: line opacities and excitation anomalies

CN proves to be a particularly useful probe of the molecular gas in PNe because of its mid-range dipole moment (μ=1.45 Debye) and its relatively strong lines, which are detected in all

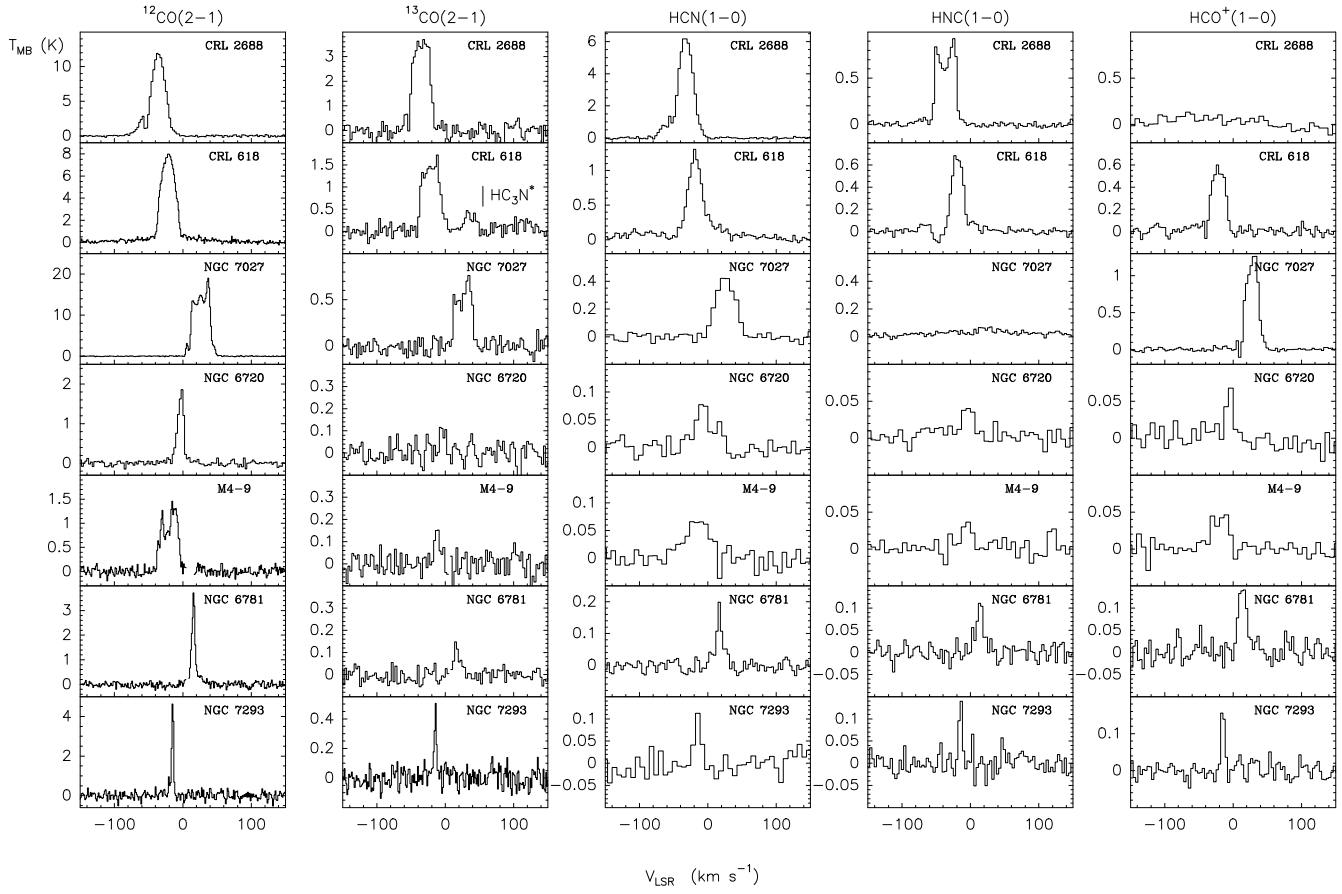

Fig. 1. J=2−1 spectra of CO and ^{13}CO, and J=1−0 spectra of HCN, HNC, and HCO$^+$ observed in the PN sample

Table 1. Properties of the observed PNe

	CRL 2688	CRL 618	NGC 7027	NGC 6720	M4–9	NGC 6781	NGC 7293	Refs
PK	...	166–6°1	84–3°1	63+13°1	24+5°1	41–2°1	36–57°1	
α_{1950} (center)	21:00:19.9	04:39:33.8	21:05:09.4	18:51:43.7	18:11:39.0	19:16:01.9	22:26:54.8	
δ_{1950} (center)	36:29:45	36:01:15	42:02:03	32:57:56	–05:00:18	06:26:46	–21:05:41	
Distance (kpc)	1.0	1.8	0.70	0.65	1.8	0.7	0.16	1
$R_{\rm i}$ (pc)^a	...^{b}	0.002	0.017	0.11	0.19	0.18	0.30	1
N/O	...	0.79	0.47	0.31	...	0.51	0.40	2
$M_{\rm m}/M_{\rm i}$^{c}	...^{b}	500	10	0.3	0.9	1.0	0.2	3
V_0 (CO) (km s^{-1})	–35	–22	26	–2	–15	17	–24	3,4
$V_{\rm exp}$ (CO) (km s^{-1})	19^d	18^d	23	22	17	22	24	3,4
Observed position	(0,0)	(0,0)	(0,0)	(–40″,–20″)	(0,+20″)	(10″,60″)	(–372″,0)	
$V_{\rm peak}$ (CO) (km s^{-1})^e	–35.6	–21.5	$\sim$ 27	$\sim$–3.0	–18.3	15.5	–15.0	
ΔV (CO) (km s^{-1})^e	60^d	40^d	45	20	40	26	8	

(1) Acker et al. (1992)
(2) from the compilation of Huggins & Healy (1989)
(3) Huggins et al. (1996), and references therein
(4) Loup et al. (1993)
(a) radius of main ionized component
(b) no ionized component
(c) mass ratio of molecular/ionized gas
(d) value for the main CO component which is superimposed on a broad (ΔV $>$ 100 km s^{-1}) emission plateau
(e) CO velocity and velocity range at the observed position

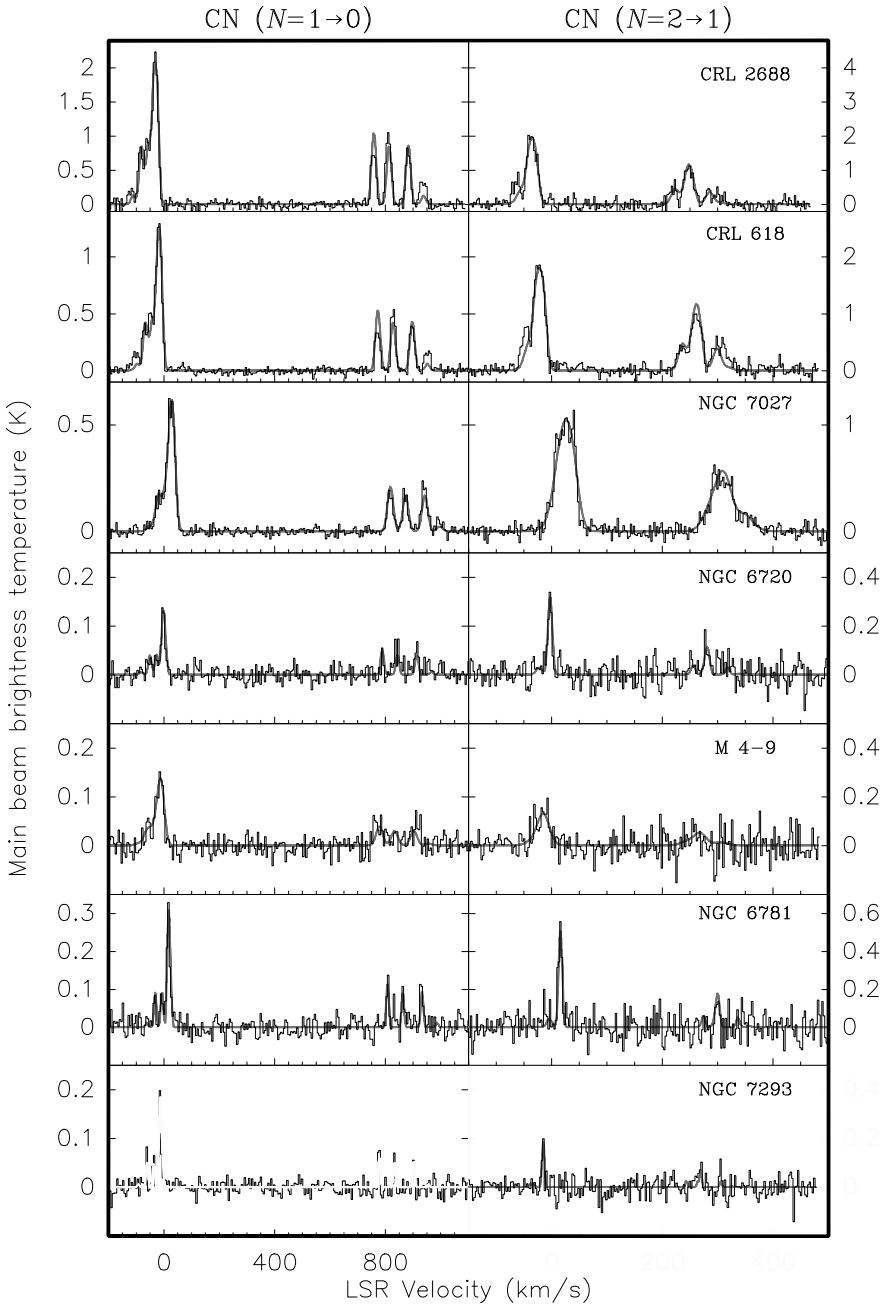

Fig. 2. N=2−1 and N=1−0 spectra of CN observed in the PN sample. The dashed profiles are fits to the observations (see text for details)

the program objects. In addition, the fine and hyperfine structure in the rotational spectrum (due to the electronic and nuclear spins: S=1/2, I=1) provide a handle on the line opacity. The line splitting distributes the line opacity among many components, and if the stronger components saturate, the line opacity can in principle be determined by comparing the relative intensities of the observed components with their intrinsic line strengths.

The N=1−0 transition of CN consists of 9 hyperfine components forming two fine-structure groups (J = 3/2 − 1/2 and J = 1/2 − 1/2) which can be seen in Fig. 2. The N=2−1 and 3−2 transitions consist of 18 and 19 hyperfine components, respectively, each transition forming three groups, of which we observed the two strongest (Figs. 2 and 4), with 93 % and 97 % of the intrinsic line strength, respectively. If we denote by R the ratio of the integrated intensities of the high-frequency (A_{high}) and low-frequency (A_{low}) fine-structure groups, i.e., $R = A_{high}/A_{low}$, the intrinsic intensity ratios that would be obtained in the case of optically-thin LTE line emission are: $R(1-0)$ = 2.0, $R(2-1)$ = 1.8, and $R(3-2)$ = 1.4. The measured values provide an estimate of the departures from these conditions. In the youngest objects with the strongest lines, CRL 2688, CRL 618, and NGC 7027, the observed values are below the intrinsic values: $R(1-0)$ ranges from 1.3 to 1.8, and $R(2-1)$ from 1.2 to 1.6. The strongest CN line components thus appear to have moderate opacity in these three objects. They are proba-

bly thinner in the evolved objects, although the weaker CN lines prevent an accurate measurement of the low frequency group.

In order to examine this in more detail, we have computed synthetic CN spectra to fit the observed line profiles using a technique previously used for NH_3 and CN spectra in AGB stars by Bachiller et al. (1987) and Bachiller et al. (1996). The analysis uses the same intrinsic linewidth for each component, with the relative line strengths and velocity spacings corresponding to the fine and hyperfine structure. The parameters of the fit are (i) the summed opacity of all hyperfine components τ_{tot}, (ii) the intrinsic linewidth, (iii) the central velocity of the main hyperfine component, and (iv) the product $X = \tau_{tot}(T_{ex} - T_{bg})$. This particular parameter combination has the advantage that the profile depends only on parameters (ii)–(iv) when the line is optically thin. The results of the fits are superposed on the observed spectra in Figs. 2–4. CRL 2688, CRL 618, and NGC 7027 are found to have moderate opacities; the values of the *total* opacities are, respectively, 4.4, 2.6, and 1.2, for the $1-0$ line, and 3.4, 4.3, and 2.0 for the $2-1$ line. The formal uncertainties of the fits are ± 0.2. Approximately half of this *total* opacity is in the main peak of the higher-frequency fine-structure group, and the moderate opacity of this peak means that the peak intensity is saturated by typically 30–50 % in these three objects. In the more evolved PNe the S/N ratio of the lower-frequency fine structure group is too poor to determine precise values for the opacities, but we are able to estimate upper limits for the total opacity of τ_{tot} <1–2 for both the $1-0$ and the $2-1$ lines. Thus in these PNe the spectra are consistent with optically thin emission.

Some differences between the observed and synthetic profiles deserve comment: (1) In CRL 2688 and CRL 618, the observed profiles are more complex than the synthetic profiles. In particular, the blueshifted parts of the strongest hyperfine groups consist of a mixture of absorption and emission. The absorption features at relatively high blue-shifted velocities are likely to arise from the approaching part of the fast bipolar winds present in both objects. Similar features are seen in the profiles of other molecular lines (e.g., Cernicharo et al. 1989; Martín-Pintado & Bachiller 1992). (2) In NGC 7027, the observed profiles deviate significantly from gaussians. The observed profiles have flatter tops with two or three peaks, which are probably due to the complex structure of the envelope (Cox et al. 1997). (3) In all three objects, the low-frequency group (J=1/2−1/2) of the N=1−0 line show strong hyperfine anomalies (see Fig. 3). In CRL 2688 and CRL 618, the intensity ratio of the outer components $r = A(F = 3/2 - 3/2)/A(F = 1/2 - 1/2)$ is observed to be 1.8, a factor 5.5 lower than the intrinsic LTE value $r = 10$. (4) In the four evolved PNe observed in the N=3−2 line, the observed intensity ratio $R(3-2)$ is $\gtrsim$2.7, well above the LTE value of 1.4.

Hyperfine anomalies are not unusual in the millimeter emission lines of species such as NH_3, N_2H^+, and HCN in interstellar clouds and circumstellar envelopes (Guilloteau & Baudry 1981; Walmsley et al. 1982; Cernicharo et al. 1984). The anomalies are generally due to one or more of the following effects: saturation of the strongest components, overlapping components, or some

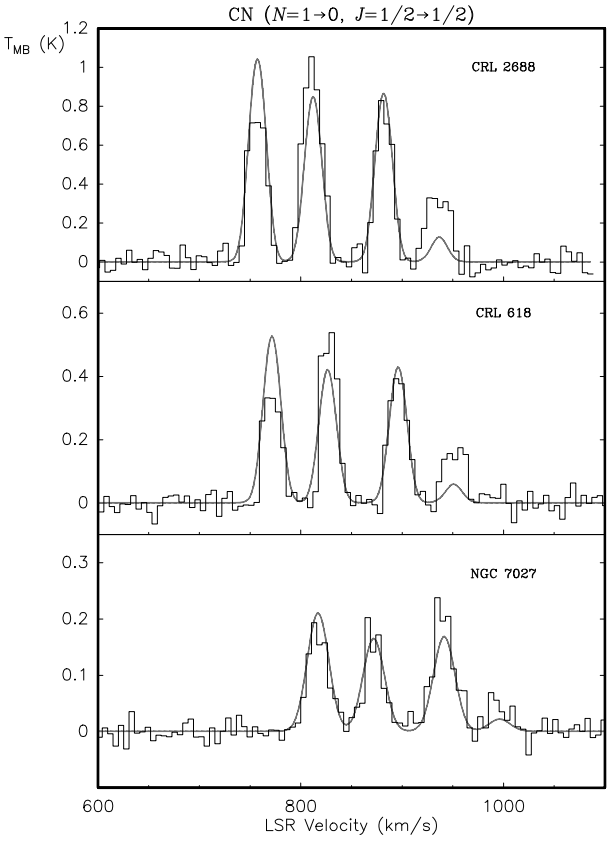

Fig. 3. Details of the J= 1/2−1/2 fine-structure group of components in the CN N=1−0 spectra. The dashed profiles are fits to the observations (see text for details). The outer components in the spectra of CRL 2688 and CRL 618 exhibit hyperfine anomalies

selective excitation effects in the radiative transfer. In the cases discussed here, the opacity effects are probably unimportant, since the $F = 3/2 - 3/2$ component has only 12 % of the total $1-0$ opacity, which itself is quite moderate, as discussed above. The fact that the most severe anomalies are observed toward the two strongest infrared sources (CRL 2688 and CRL 618) suggests that the anomalies are due to radiative pumping through the IR bands near 4.9 μm (the vibrational v=1−0 band) and 1.1 μm (the CN "red system" to the excited low-lying $^2\Pi$ electronic state). Excitation anomalies have been reported in the CN line emission from AGB stars (Olofsson et al. 1993; Bachiller et al. 1996) and are also thought to be due to the near-IR pumping. We note that no comparable anomalies in the value of r are observed in the evolved PNe such as the Helix (even though the S/N ratio of the $1-0$ spectra is sufficient that they would be seen), which we attribute to the CN excitation being purely collisional (see below).

The fine structure anomalies seen in the N=3−2 profiles are likely to be excitation effects due to the properties of the CN collisional rates, although no theoretical values of the collisional coefficients are available with which to test this. Given the high interest in the CN molecule as a diagnostic of the physical conditions of both interstellar and circumstellar molecular gas,

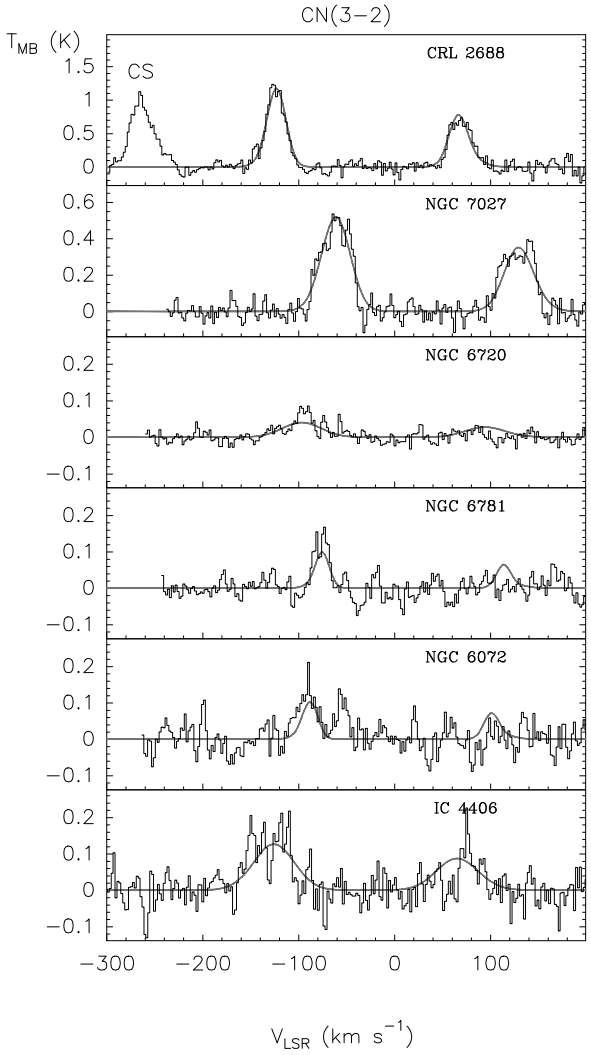

Fig. 4. N=3−2 spectra of CN observed with the CSO. The dashed profiles are fits to the observations (see text for details). The strong line seen at negative velocities in the spectrum of CRL 2688 is CS J=7−6 in the image side band

the computation of the collisional coefficients for CN would be very valuable.

3.2. Excitation and physical conditions

Estimates of the excitation temperatures of the molecules are needed to determine molecular column densities from the observations, and, if the excitation is dominated by collisions, it also provides useful constraints on the physical conditions in the gas. In order to study the importance of collisions we have compared the upward collisonal rates for low lying rotational levels with the radiative pumping which results from the absorption and subsequent emission of near infrared radiation in the vibration-rotation bands. This latter effect is important in typical AGB envelopes (Morris 1975), but the circumstances in proto-PNe and PNe are somewhat different: the densities in the shells are relatively high, and as the nebula evolves, the near infrared radiation field shifts to longer wavelengths and then decreases rapidly in intensity with the decreasing luminosity of the central star. To estimate collision rates we use a representative temperature of 25 K, a mass-loss rate of 10^{-4} $M_\odot$ yr^{-1}, and a cross section of 2×10^{-15} cm^{-2}, which provides a good approximation to detailed collisional calculations. For the radiative pumping rates, we estimate the radiation field in the envelopes at the wavelengths of the vibrational bands of the molecules, using the observed infrared fluxes of the program PNe. We find that radiative pumping is dominant only in the proto-PNe for species with transitions at longer wavelengths (e.g., HCN), and negligible in the more evolved PNe, especially in cases like the Ring or the Helix, which have high density clumps well separated from low luminosity central stars.

The CO excitation temperature, $T_{\rm ex}$, and the gas kinetic temperature, $T_{\rm K}$, can be estimated from the 2−1/1−0 intensity ratio of the ^{13}CO lines, since these lines are optically thin and they are easily thermalized, so that $T_{\rm ex}$ is a good estimate of $T_{\rm K}$. If we assume that the emitting region fills the antenna beam in both lines, or that the beam filling factor is the same (e.g., for an extended clumpy medium), the derived excitation temperatures are typically in the range 25–60 K for the PNe and the proto-PNe. These values probably overestimate the actual values of $T_{\rm ex}$ since the observations are made towards a peak in the emission. On the other hand, strict lower limits to $T_{\rm ex}$ can be obtained by considering the extreme case of a point source unresolved by both beams, in which case the derived excitation temperatures are $>$6–10 K. CO maps show that the actual situation is closer to the first case than to the second, and we adopt $T_{\rm K}$=25 K as a representative value for all objects. This value is in agreement with estimates obtained from extensive ^{12}CO mapping of PNe, including NGC 6720 and NGC 6781, in which complete maps in the 1−0 and 2−1 lines allow detailed study of the line ratio on the same angular scale over the whole nebula (Bachiller et al. 1989ab, 1993).

In addition to CO, rotational temperatures can be estimated for CN and HCO$^+$, for which we also have multiline observations. Assuming optically thin emission and the same filling factors in each beam, we find typical values of $T_{\rm ex}$ in the range 5–10 K in all the observed objects. Higher excitation is indicated by strong HCO$^+$ (3−2) emission seen in NGC 7027 with the small beam of the 30-m telescope, but in this case differential beam dilution is probably partly or fully responsible. The values derived for CN from the 3−2/1−0 ratio are particularly useful, since the observations for these lines were made with beams of the same angular size; the corresponding values of $T_{\rm ex}$ are close to 10 K for NGC 6781, NGC 6720, and NGC 7027. Taking into account the modest opacities in the CN lines make little difference. These lower values of $T_{\rm ex}$ for CN and HCO$^+$ compared to CO are not unexpected because of their higher dipole moments, and their subthermal excitation provides a means of roughly estimating the densities in the gas.

To estimate the densities in the gas, we have carried out radiative transfer calculations using the LVG approximation. The numerical code for CN, developed by Fuente et al. (1995),

uses the collisional rates of CS (Green & Chapman 1978) corrected for the different molecular sizes, and takes into account the CN fine and hyperfine splitting. These rates are not accurate enough for investigating collisional excitation anomalies among the fine and hyperfine components, as observed in the 3−2 line, but they are expected to be adequate for predicting a critical density for each line, and thus for making useful estimates of the gas densities. Based on the results described above, we assumed a kinetic temperature of 25 K in the calculations, and in the conversion from observed intensities to intrinsic brightness we again considered two cases for the source size and structure. For the extreme case of a point-like source, the derived densities are 2–4 $\times$ 10^4 cm^{-3}. In the more realistic case in which the CN emitting region fills the antenna beams at both frequencies, or a clumpy medium with similar filling factors in both beams, the volume densities are 1–4 $\times$ 10^5 cm^{-3}. These values apply to both the PNe and the proto-PNe.

Values (and limits) for the densities derived from similar calculations for HCO$^+$ (for which we have 1−0 and some 3−2 observations) are fully compatible with the estimates from CN in NGC 6781, NGC 7293, and NGC 6720. In NGC 7027 the strong 3−2 line seen with the 30-m telescope leads to densities in excess of 10^6 cm^{-3}, although as noted above, these observations may need to take into account beam dilution effects. In any event, the parameters estimated for the proto-PNe and NGC 7027 must be considered only as rough averages, since the observations sample substantial parts of relatively complete envelopes and large ranges in both density and temperature are expected. In the more extended PNe where the shells are spatially well resolved, the parameters estimated here will refer to the conditions in the molecular clumps which make up the shells.

4. Molecular abundances

4.1. Column densities

In order to determine the molecular abundances we first estimate the column densities using the simplifying assumptions of optically thin emission and thermal equilibrium. We then indicate how these estimates should be modified, based on our discussion of the physical conditions given above.

Table 3 lists the column densities derived from the observed line intensities assuming optically thin emission with the rotational levels thermalized at a uniform temperature of 25 K. As discussed above, this temperature is appropriate for CO, but will not be strictly valid for species such as HCN, HNC, HCO$^+$, and CN. These molecules have much larger dipole moments ($\mu \sim$ 1.4–3 Debye) compared to CO (μ = 0.11 Debye), so that their rotational populations will be sub-thermal for the volume densities expected in the nebular gas. For more representative values of excitation temperatures in the range 6–10 K indicated by the radiative transfer simulations described above, the column densities of these species should be divided by a factor of $\sim$2. In any case, apart from opacity effects, the column density ratios HCN/HNC/HCO$^+$/CN should provide robust estimates of the actual abundance ratios since the frequency of the observed lines, the level structures, and the dipole moments are not very different for these species. The simulations indicate that the CO and HCN lines are optically thick in the most massive envelopes (CRL 2688, CRL 618, NGC 7027), so the column densities quoted for these in Table 3 are lower limits. On the other hand, the CN emission has only moderate opacities in these objects, and all the lines are close to optically thin in the more evolved PNe. Thus apart from the limitations mentioned here, the simplified estimates given in Table 3 should provide useful estimates of the abundances in the molecular gas.

Fig. 5 shows how the CN, HCN, HNC, HCO$^+$, and CS abundances vary among the observed sample, which have been ordered according to their degree of evolution, as discussed further below. The left hand axis indicates abundances relative to ^{13}CO, and the right hand axis indicates abundances relative to H_2, assuming a representative ^{13}CO abundance of 2.5 $\times$ 10^{-5}, although we caution that the abundances of CO and ^{13}CO are not well known and are difficult to estimate in these regions. CS, HC_3N, SiO, and SiC_2 are well detected in the two proto-PNe, but they are not detected in the PNe; their abundances vary from CRL 2688 to CRL 618 and NGC 7027 in a similar way, so only the CS abundance has been shown in the figure as representative of the others.

Overall, the abundances show distinct evolutionary trends. In particular, the short transition from proto-PN to PN is accompanied by the destruction of CS, HC_3N, SiO, and SiC_2, and the production of a relatively large abundance of HCO$^+$, as well as an enhancement of CN. After this, however, the observed abundances in the PNe remain approximately the same even though they span a large range in evolution.

4.2. The CO/^{13}CO ratio

The LVG radiative transfer simulations indicate that the column densities of both CO and ^{13}CO are relatively well determined for the evolved PNe. Both lines of the two isotopes remain optically thin and thermalized even when the assumed kinetic temperature and density are varied beyond the expected range, confirming that the LTE assumption is valid in these cases. The column densities listed in Table 3 were computed from the 2−1 intensities for an excitation temperature of 25 K, but, as discussed by Huggins & Healy (1989), they are valid to within a factor of 2 over a large range of temperatures. In any case, the small temperature dependence cancels out when the CO/^{13}CO isotopic ratio is formed.

The observed CO/^{13}CO ratios are around 20 for the evolved PNe, except for the Helix where the observed ratio is close to 10. These and the values previously measured toward NGC 2346 (Bachiller et al. 1989b) and IC 4406 (Cox et al. 1992) indicate that in evolved PNe 10 $\lesssim$ CO/^{13}CO $\lesssim$ 25. An important question is whether this ratio is the same as the atomic C/^{13}C ratio. In principle, selective photodissociation could modify the molecular ratio from the elemental C/^{13}C ratio, since ^{13}CO is self-shielded less efficiently than CO. However, the destruction of ^{13}CO is expected to be compensated by the isotopic exchange

Table 2. Integrated intensities of the observed molecular lines (in K km s^{-1})

		CRL 2688	CRL 618	NGC 7027	NGC 6720	M4–9[e]	NGC 6781[e]	NGC 7293
^{12}CO	$J = 2\rightarrow1$	312.5 (1.3)	182.2 (1.1)[c]	448.7 (0.6)	20.0 (0.4)	32.2 (0.5)	28.4 (0.6)	17.5 (0.7)
^{13}CO	$J = 1\rightarrow0$	35.4 (0.6)	13.7 (0.3)	6.4 (0.3)	0.27 (0.11)	0.6 (0.2)	0.32 (0.14)	0.67 (0.09)
^{13}CO	$J = 2\rightarrow1$	112 (3)	41.2 (1.3)	17.3 (0.8)	0.9 (0.3)	1.8 (0.4)	1.7 (0.2)	1.8 (0.2)
CN	$N = 1\rightarrow0$[a]	97 (2)	54.2 (0.6)	25.1 (0.4)	3.9 (0.3)	6.4 (0.4)	7.0 (0.4)	2.7 (0.2)
CN	$N = 2\rightarrow1$[b]	58 (2)	53.1 (0.8)	41.9 (0.6)	4.5 (0.7)	4.5 (0.3)	4.6 (0.5)	1.0 (0.2)
CN	$N = 3\rightarrow2$[d,f]	29.0 (0.5)		17.9 (0.5)	2.8 (0.3)		2.6 (0.3)	
HCN	$J = 1\rightarrow0$	177 (1)	26.2 (0.7)	14.3 (0.4)	3.2 (0.2)	2.8 (0.3)	2.4 (0.2)	1.6 (0.2)
HNC	$J = 1\rightarrow0$	26.7 (0.3)	12.9 (0.4)	1.0 (1.2)	0.74 (0.10)	0.62 (0.13)	1.65 (0.15)	0.80 (0.11)
HCO$^+$	$J = 1\rightarrow0$	(0.7)	13.1 (0.4)	26.5 (0.2)	0.86 (0.11)	1.25 (0.12)	2.2 (0.2)	0.89 (0.10)
HCO$^+$	$J = 3\rightarrow2$			76 (5)	(1.3)		0.33 (0.05)[d]	(0.06)[d]
CS	$J = 3\rightarrow2$	43[g]	4.8 (0.3)	(0.3)	(0.13)	(0.2)	(0.2)	(0.08)
HC_3N	$J = 16\rightarrow15$	67.5 (0.6)	20.6 (0.5)	(0.3)	(0.11)	(0.2)	(0.2)	(0.11)
SiO	$J = 3\rightarrow2$	9.0 (0.4)	2.1 (0.2)	(0.13)	(0.11)	(0.14)	(0.15)	(0.17)
SiC_2	$J = 6_{06}\rightarrow5_{05}$	5.7 (0.6)	1.3 (0.6)	(0.3)	(0.15)	(0.3)	(0.15)	(0.14)

Notes: Values in parentheses are 1 r.m.s. errors and upper limits. Upper limits are calculated at 1 r.m.s., and assuming the emission intervals (ΔV) given in Table 1 for each observed position. [a] The quoted value refers to the high frequency fine-structure group ($J = 3/2\rightarrow1/2$). [b] The quoted value refers to the high frequency fine-structure group ($J = 5/2\rightarrow3/2$). [c] This value does not include the very high velocity wings. [d] Measured at the CSO telescope. [e] Obvious interstellar contamination has been subtracted from the spectra. [f] The quoted value refers to the high frequency fine-structure group ($J = 7/2\rightarrow5/2$). [g] Data from Bujarrabal et al. (1988)

Table 3. Abundance ratios and ^{13}CO column densities

	CRL 2688	CRL 618	NGC 7027	NGC 6720	M4–9	NGC 6781	NGC 7293
N(^{13}CO) (cm^{-2})	$5.5\,10^{16}$	$2.1\,10^{16}$	$9.1\,10^{15}$	$4.3\,10^{14}$	$9.1\,10^{14}$	$6.9\,10^{14}$	$9.6\,10^{14}$
Abundances with respect to ^{13}CO							
^{12}CO/^{13}CO	>3	>4	>25	23	18	20	9.3
CN/^{13}CO	0.022	0.031	0.033	0.109	0.085	0.122	0.033
HCN/^{13}CO	>0.009	>0.004	>0.005	0.022	0.009	0.010	0.005
HNC/^{13}CO	0.002	0.002	$3\,10^{-4}$	0.005	0.002	0.007	0.003
HCO$^+$/^{13}CO	$<3\,10^{-5}$	0.0015	0.007	0.005	0.003	0.008	0.002
CS/^{13}CO	0.003	$9\,10^{-4}$	$<1.2\,10^{-4}$	<0.001	$<8\,10^{-4}$	<0.0011	$<3\,10^{-4}$
HC_3N/^{13}CO	0.008	0.006	$<2.1\,10^{-4}$	<0.002	<0.0014	<0.002	$<7\,10^{-4}$
SiO/^{13}CO	$3\,10^{-4}$	$1.8\,10^{-4}$	$<2.5\,10^{-5}$	$<4\,10^{-4}$	$<3\,10^{-4}$	$<4\,10^{-4}$	$<3\,10^{-4}$
SiC_2/^{13}CO	$6\,10^{-4}$	$4\,10^{-4}$	$<2.0\,10^{-4}$	<0.002	<0.002	<0.0013	$<9\,10^{-4}$

reaction ^{12}CO+^{13}C$^+\rightarrow^{13}$CO+^{12}C$^+$ which is faster than the ^{13}CO photodestruction for conditions typical of the edges of PN envelopes (Likkel et al. 1988). The kinetic temperature is also high enough that isotopic fractionation is not expected to operate. Thus the observed CO/^{13}CO ratio is likely to reflect the C/^{13}C ratio.

The isotopic C/^{13}C ratio in the evolved PNe appears to be significantly lower than the Solar System value of 89, and within the large range (typically ∼10–50) found for the envelopes of AGB stars (Knapp & Chang 1985; Wannier & Sahai 1987; Kahane et al. 1988). The best determination, measured through several molecular transitions, is for the envelope of IRC+10216, where C$/^{13}$C ∼ 47 (Kahane et al. 1988).

The value of the C/^{13}C ratio in the gas is expected to be related to the abundance of ^{3}He which, together with that of deuterium, is a basic parameter to test cosmological nucleosynthesis models (e.g. Galli et al. 1995). There is increasing evidence for important discrepancies between the measured abundance of ^{3}He and that predicted by standard chemical models (e.g., Olive et al. 1995). To avoid such discrepancies, it has been recently suggested that a non-standard mixing mechanism operates on the red giant branch for stars of mass up to $\sim 2\,M_\odot$ and suppresses the production of ^{3}He (Charbonnel 1995). An unavoidable consequence of this mixing is that the ^{3}He destruction is always accompanied by a decrease in the C/^{13}C ratio. For instance, in the case of a $1\,M_\odot$ star, the predicted isotopic ratio is about 5, whereas "standard" models predict a value of $\sim$ 25. Some PNe, including NGC 6720, have been recently observed to have high ^{3}He abundances (see Olive et al. 1995, and references therein). So it is interesting to note that the values

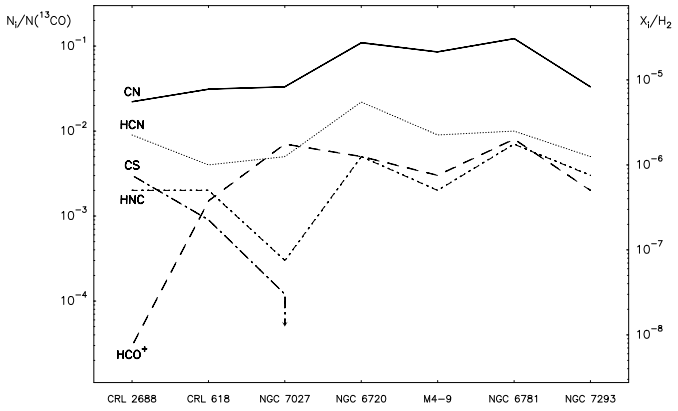

Fig. 5. Molecular abundances in the PN sample. The left hand scale indicates abundances relative to ^{13}CO. The right hand scale indicates abundances relative to H_2, for an assumed ^{13}CO abundance of 2.5×10^{-5}

we find for the C/^{13}C ratio are correspondingly high ($\sim$ 20) in most nebulae, suggesting that the non-standard mixing mechanisms were not at work in these objects. The limits we obtain for the C/^{13}C ratio in CRL 2688, CRL 618, and NGC 7027 are poor due to the high opacity of the CO lines, but Kahane et al. (1992) measured C/^{13}C ratios higher than 30 in all three objects. This could indicate that the progenitors of all the nebulae in our sample were stars of $>2\,M_{\odot}$(except perhaps the Helix which seems to present a lower C/^{13}C ratio). Further measurements of the ^{3}He abundances in these objects would be a useful test of the validity of the non-standard mixing mechanisms.

5. Discussion

5.1. Physical and chemical evolution of the envelopes

The molecular envelopes discussed in this paper range from radially extended, relatively complete circumstellar envelopes (CRL 2688 and CRL 618) to large, thin, fragmented shells or rings (NGC 6781 and NGC 7293). The major structural differences between the envelopes can be ascribed mainly to evolutionary effects, and the nebulae have several basic features in common (including density enhancements towards an equatorial plane, moderate or high N/O values, and C/O ratios > 1 for those in which it is measured) which suggest they are roughly similar kinds of objects at different stages of development. Accordingly, the envelopes have been ordered in Fig. 5 in an approximate time sequence, based on the size of the ionized nebulae and the radio continuum surface brightness. A similar order is obtained using temperature and luminosity estimates of the central stars. The post AGB kinematic timescales of the envelopes ($R_{\rm i}/V_{exp}$, see Table 1) range from $\lesssim$ a few 100 yr for the proto-PNe to $\sim$10,000 yr for NGC 7293, and the mass ratio of molecular/ionized gas (Table 1) decreases dramatically along the sequence in line with the discussion of envelope evolution given by Huggins et al. (1996).

A key result on the physical state of the gas that emerges from our multi-line observations of the envelopes is that, once the PNe have formed, the density of the surviving molecular gas remains high. Our best estimates for the densities in the evolved PNe are $\sim$ few $\times\,10^5$ cm^{-3}. These densities are much higher than the typical electron densities of 100–800 cm^{-3} determined from optical forbidden line ratios (see, e.g., Stanghellini & Kaler 1989), and are consistent with the idea that the ionized gas and the cool, dense molecular gas are roughly in pressure equilibrium. High resolution imaging in CO (Bachiller et al. 1993), H_2 (e.g., Kastner et al. 1996), and at optical wavelengths (e.g., O'Dell & Handron 1996), indicates that the envelopes of the evolved PNe are extremely clumped. Thus our density estimates refer to the clumps that make up the shell structures at the positions observed, and in NGC 7293 they are essentially the same as estimates we made earlier for single cometary globules or small groups of them, using CO observations (Huggins et al. 1992). The high density of the neutral clumps contrasts with the common assumption that PNe rapidly become more and more diffuse as they expand. The clumping of the envelopes is one of the dominant aspects of the PNe studied here, and is essential in producing environments needed for the survival of the molecular gas.

The results of our observations reported in Table 3 and Fig. 5 indicate that significant changes in the molecular abundances take place during the evolution of the envelopes. The largest effect is the rapid increase in the abundance of HCO^+ by about two orders of magnitude during the proto-PN to PN transition. The CN abundance also increases but by a smaller factor of about 4. At the same time, the species CS, HC_3N, SiO, and SiC_2 (represented by CS in Fig. 5) decrease, and must be effectively destroyed when the planetary nebula forms. The HCN abundance appears roughly constant (HCN/^{13}CO $\sim$ 0.01), but the HCN(1$-$0) line is most likely optically thick in the younger objects, so the apparent constancy probably masks some depletion of HCN. Finally, HNC appears overabundant by a factor of 2–3 in some evolved PNe relative to the two proto-PNe, but this is only marginally significant given the uncertainties involved in the column density estimates. HNC is, however, strongly deficient in NGC 7027, causing a deep minimum for HCN at the young PN phase in Fig. 5.

It is noteworthy that the molecular abundances observed in the four evolved PNe are nearly the same, suggesting a similar chemical evolution. For these PNe, HCN, HNC, and HCO^+ have comparable abundances, but CN is about an order of magnitude more abundant. On average, including previous measurements in NGC 2346 (Bachiller et al. 1989b), NGC 6072, and IC 4406 (Cox et al. 1992), we find that CN/HCN = 9, HNC/HCN = 0.5, and HCO^+/HCN = 0.5 in the evolved PNe. These CN/HCN, HNC/HCN, and HCO^+/HCN ratios are enhanced by one, two, and three orders of magnitude, respectively, over the values observed in the prototypical AGB envelope IRC+10216 (Omont 1993).

5.2. Chemical processes

The main processes which are thought to determine the chemical composition of the molecular gas in PNe have been extensively discussed by Cox et al. (1992). Here we update the discussion in the light of our new observations and some model calculations reported by Howe et al. (1992, 1994).

The most important influence on the chemistry is almost certainly the ultraviolet radiation field of the central star. During the transition from proto-PN to young PN, the ultraviolet radiation field incident on the inner surface of the molecular gas rises rapidly to very high values ($\chi \sim 10^5$, in units of the average interstellar field) and then steadily decreases because of the expansion of the envelope and the decrease in luminosity of the central star ($\chi \sim 10 - 100$ in the most evolved PNe). The ultraviolet radiation creates photo-dominated regions (PDRs) in the neutral gas (Hollenbach & Natta 1995), similar to those in interstellar clouds (e.g., Tielens & Hollenbach 1985; Hollenbach et al. 1991). In these regions, photo-dissociation and a high level of ionization play important roles in the chemistry, although no detailed thermal-chemical models have yet been developed for the carbon-rich case which is most relevant here. PDRs have been detected in PNe through the emission of atomic fine structure lines, e.g., the ground state line of C I in NGC 6720 (Bachiller et al. 1994), and O I, C I, and C II in NGC 7027 (Liu et al. 1996; Young et al. 1996, and references therein). The existence of molecules in the PDR gas rests heavily on the presence of high density gas, which is confirmed by the multi-line observations reported here. In homogeneous, expanding envelopes, the gas becomes optically thin and diffuse on short timescales, and is rapidly photo-dissociated.

A second, potentially important influence on the chemistry is the effect of shocks which compress and heat the molecular gas making possible some endothermic reactions. The problem in evaluating the importance of shocks is that the dynamical history of the gas is not known in detail. High velocity molecular flows are in fact seen in CRL 2688 and CRL 618, but they are largely confined to the bipolar lobes and probably do not significantly affect the bulk of the gas observed here. Shocks are also an integral part of the commonly discussed two wind model, in which a fast ionized wind from the central star is believed to form the PN shell. This situation has been modeled by Howe et al. (1992) who find that the reformation of molecules in the shocked gas leads only to the synthesis of small molecules and ions such as CH, CH_2, and CH_3^+, and not the heavier species detected here. It is conceivable that shock chemistry is more effective under different conditions than assumed, e.g., in the presence of clumps, but this remains to be explored.

The large abundance of CN that we observe in PNe is entirely consistent with the effects of chemistry dominated by ultraviolet radiation. The CN/HCN ratio is about 0.5 in C-rich AGB envelopes (Bachiller et al. 1996), $\lesssim$2 in CRL 2688 and $\lesssim$8 in CRL 618 (the limits are because HCN is probably optically thick in these two objects), and $\sim$9 in evolved PNe. The CN in AGB envelopes is produced in the outer regions through the HCN photochain by ambient ultraviolet radiation. As the stellar radiation turns on inside, a general increase in the CN/HCN ratio will occur as a result of the photoionization of the HCN-rich inner envelope, and locally in the gas, mainly as a result of the smaller effective photo-dissociation rate for CN by a factor of 2–3. Howe et al. (1994) have constructed simple, steady state chemical models for the globules in the Helix which should be roughly applicable to all the evolved PNe studied here. The predicted CN/HCN ratio and the CN/H_2 abundance for the C-rich case are in rough qualitative agreement with our observations (within factors of 3–10) and lend support to this general picture.

HNC is formed in C-rich AGB envelopes and in the interstellar medium from dissociative recombination of $HCNH^+$ (Glassgold et al. 1987). A similar mechanism is probably responsible for HNC in the PNe, and the higher HNC abundances in the more evolved objects can be ascribed to a higher level of ionization in the gas, as expected in the photon-dominated picture. The HNC/HCN ratio predicted in the globule model of Howe et al. (1994) is lower than observed by a factor of 20, but could possibly be reconciled with a change in some of the model parameters. One unexpected result for HNC is the low abundance in NGC 7027. The observed HNC/HCN ratio ranges from 0.2 to 0.7 in the evolved PNe, but is $<$0.06 in NGC 7027 (where this value is an upper limit because the HCN line is likely optically thick). One possible explanation for this lies in the temperature of the molecular gas. Large variations of a factor $\approx$100 are seen in the HNC/HCN ratio in interstellar clouds, and can be explained by the effects of the local gas temperature (Schilke et al. 1992). Simple chemical models predict that HNC/HCN decreases with temperature (as observed) and this is due to two reactions with activation energies of the order of 200 K: HNC+H $\rightarrow$ HCN +H and HNC+O $\rightarrow$ NH+CO. In the case of the PNe discussed here, NGC 7027 has the highest luminosity in energetic photons, and as a compact PN it is likely that the temperatures in the PDR gas are significantly higher than they are in the more evolved PNe where the incident radiation is less intense. Thus it seems entirely plausible that the weaker HCN emission in NGC 7027 is a result of the higher temperatures in the gas.

The most difficult of our observations to explain is the large abundance of HCO^+ which appears at the young PN phase and persists at a similar level in all the more evolved objects. The problem was first recognized in NGC 7027 (Deguchi et al. 1990) and in NGC 6072 and IC 4406 (Cox et al. 1992), and is equally apparent in NGC 7293 where the predictions of carbon-rich, low temperature globule models of Howe et al. (1994) fall below the abundance we observe by three orders of magnitude or more. Some basic aspect of the physical conditions or the chemistry is missing from the models. HCO^+ is likely formed in PNe by gas-phase reactions similar to those taking place in the interstellar medium, with the difference that the H_3^+ abundance in PNe is expected to be low due to dissociative recombination so that a large ionization rate of H_2 is necessary. One solution to this problem suggested by Deguchi et al. (1990) is the effect of soft X-ray radiation from the central star. This apparently works in NGC 7027, but is unlikely to be the correct explanation because we observe similar HCO^+ levels in much more

evolved PNe where the X-ray fluxes are lower by several orders of magnitude. The large ionization rate is more likely related to the ultraviolet radiation field and the structure of the PDR gas, but a contribution to the HCO^+ abundance generated from endothermic reactions in the shocks is also possible.

The complexity of the chemistry in PNe is underscored by the very recent detection of H_2O and OH in NGC 7027 with ISO (Liu et al. 1996). The presence of these molecules was not expected in this carbon rich environment. In a subsequent paper, Cernicharo et al. (1997) identified in the ISO far-infrared spectrum of NGC 7027 the pure rotational transitions of CH^+ and questioned the assignment of the H_2O identification. A likely explanation is that the these species (OH, CH^+, and perhaps H_2O) originate in the warm, dense molecular gas in the PDRs, although the detailed chemistry has not been explored. The presence of the above species may result from the rich ion chemistry expected in the PDR (Sternberg & Dalgarno 1995, see also Howe et al. 1992), and could well be related to the large abundance of HCO^+ that we observe.

6. Conclusions

The observations reported in this paper substantially increase the available data on the evolution of the physical and chemical conditions in the molecular envelopes of PNe. They demonstrate that a range of molecular species can survive in PNe to advanced stages of evolution (e.g., in the Helix), and they provide density estimates of the neutral clumps in which the molecular gas is found. In the evolved PNe the densities are $\sim$ few $\times\ 10^5$ cm^{-3} and the temperatures are $\sim$25 K, consistent with the idea that the clumps are roughly in pressure equilibrium with the ionized gas.

The molecular abundances derived from the observations confirm that the chemical composition of the molecular gas in PNe is different from that in the precursor AGB envelopes, and there are clear evolutionary trends. From the proto-PN to the PN phase, the abundance of HCO^+ increases by two orders of magnitude, and CN by a factor of 4. At the same time CS, HC_3N, SiO, and SiC_2 decrease, and are effectively destroyed as the PNe form. In the more evolved PNe the abundances remain relatively constant: CN is about an order of magnitude more abundant than HCN, HNC, and HCO^+, and the average abundance ratios are CN/HCN = 9, HNC/HCN = 0.5, and HCO^+/HCN = 0.5. These ratios are respectively, one, two, and three orders of magnitude higher than in the prototypical AGB envelope IRC+10216.

We do not yet have detailed models of the chemical evolution for the extreme conditions found in PNe, but most of the observed effects are consistent with a chemistry dominated by photo-dissociation and ion molecular reactions, initiated by the radiation field of the central star. The origin of the large increase in the HCO^+ abundance is less clear: it could arise from a similar chemistry and/or from shocks. Detailed mapping of the distribution of these different molecular species (already in progress) will be important in developing a more complete picture of the interaction of the neutral envelope with the ionized nebula and the central star.

Acknowledgements. Thanks are due to Dr. A. Omont for stimulating discussions on chemistry. R.B. acknowledges partial support from Spanish DGICYT grant PB93–48, and P.J.H. from NSF grant AST-9314408. R.B. also acknowledges hospitality at the Observatoire de Grenoble where part of this paper was written. The CSO is supported by the NSF under grant AST-9313929.

References

Acker A, Ochsenbein F, Stenholm B, Tylenda R, Marcout J, Schohn C. 1992, Strasbourg-ESO catalog of galactic planetary nebulae, ESO, Garching
Bachiller R, Guilloteau S, Kahane C. 1987, A&A 173, 324
Bachiller R, Gómez-González J, Bujarrabal V, Martín-Pintado J. 1988, A&A 196, L5
Bachiller R, Bujarrabal V, Martín-Pintado J, Gomez-Gonzalez J. 1989a, A&A 218, 252
Bachiller R, Planesas P, Martín-Pintado J, Bujarrabal V, Tafalla M. 1989b, A&A 210, 366
Bachiller R, Huggins PJ, Cox P, Forveille T. 1993, A&A 267, 177
Bachiller R, Huggins PJ, Cox P, Forveille T. 1994, A&A 281, L93
Bachiller R, Fuente A, Bujarrabal V, Colomer F, Loup C, Omont A, de Jong T. 1996, A&A, in press
Bujarrabal V, Gomez-Gonzalez J, Bachiller R, Martin-Pintado J. 1988, A&A 204, 242
Cernicharo J, Castets A, Duvert A, Guilloteau S. 1984, A&A 139, L13
Cernicharo J, Guélin M, Martín-Pintado J, Peñalver J, Mauersberger R. 1989, A&A 222, L1
Cernicharo J, Liu X, González-Alfonso E. et al. 1997, submitted to A&A
Charbonnel C. 1995, ApJ 453, L41
Cox P, Guesten R, Henkel C. 1988, A&A 181 L19
Cox P, Huggins PJ, Bachiller R, Forveille T. 1991, A&A 250, 533
Cox P, Omont A, Huggins PJ, Bachiller R, Forveille T. 1992, A&A 266, 420
Cox P, Bachiller R, Huggins PJ, Omont A, Guilloteau S. 1993, in Planetary Nebulae, eds R. Weinberger & A. Acker, Kluwer, p227
Cox P, et al. 1997, in preparation
Deguchi S, Izumiura H, Kaifu N, Mao X, Nguyen-Q-Rieu, Ukita N. 1990, ApJ 351, 522
Forveille T, Huggins PJ. 1991, A&A 248, 599
Fuente A, Martín-Pintado J, Gaume R. 1995, ApJ 442, L33
Galli D, Palla F, Ferrini F, Penco U. 1995, ApJ 443, 536
Glassgold AE, Mamon GA, Omont A, Lucas R. 1987, A&A 180, 183
Green S, Chapman S. 1978, ApJS 37, 169
Guilloteau S, Baudry A. 1981, A&A 97, 213
Hollenbach DJ, Natta A. 1995, ApJ 455, 133
Hollenbach DJ, Takashashi T, Tielens AGGM. 1991, ApJ 377, 192
Howe DA, Millar TJ, Williams DA. 1992, MNRAS 257, 419
Howe DA, Hartquist TW, Williams DA. 1994, MNRAS 271, 811
Huggins PJ, Healy AP. 1989, ApJ 346, 201
Huggins PJ, Bachiller R, Cox P, Forveille T. 1992, ApJ 401, L43
Huggins PJ, Bachiller R, Cox P, Forveille T. 1996, A&A, in press
Kahane C, Gómez-González J, Cernicharo J, Guélin M. 1988, A&A 190, 167
Kahane C, Cernicharo J, Gómez-González J, Guélin M. 1992, A&A 256, 235
Kastner JH, Weintraub DA, Gatley I, Merrill KM, Probst RG. 1996, ApJ 462, 777
Knapp GR, Chang KM. 1985, ApJ 293, 281
Latter WB, Walker CK, Maloney PR. 1993, ApJ 419, L97

Likkel L, Forveille T, Omont A, Morris M. 1988, A&A 198, L1
Liu XW, Barlow MJ, Nguyen-Q-Rieu et al. 1996, A&A, ISO volume
Loup C, Forveille T, Omont A, Paul JF. 1993, A&AS, 99, 291
Martín-Pintado J, Bachiller R. 1992, ApJ 391, L93
Mauersberger R, Guélin M, Martín-Pintado J, Thum C, Cernicharo J, Hein H, Navarro S. 1989, A&ASS 79, 217
Morris M. 1975, ApJ 197, 603
O'Dell CR, Handron KD. 1996, AJ 111, 1630
Olive KA, Rood RT, Schramm DN, Truran J, Vaugioni-Flam E. 1995, ApJ 444, 680
Olofsson H, Johansson L, Nguyen-Q-Rieu, Sopka B, Zuckerman B. 1982, BAAS 14, 895
Olofsson H, Eriksson K, Gustafsson B, Carlström U. 1993, ApJS 87, 305
Omont A. 1993, J. Chem. Soc. Faraday Trans. 89, 2137
Sahai R, Wootten A, Clegg RES. 1991, A&A 251, 560
Sahai R, Wootten A, Schwarz H, Wild W. 1994, ApJ 428, 237
Schilke P, Walmsley CM, Pineau des Forêts G, Roueff E, Flower DR, Guilloteau S. 1992, A&A 256, 595
Stanghellini L, Kaler JB. 1989 ApJ 343, 811
Sternberg A, Dalgarno A. 1995 ApJSS 99, 565
Thronson HA, Bally J. 1986, ApJ 300, 749
Tielens AGGM, Hollenbach DJ. 1985, ApJ 291, 722
Truong-Bach, Morris D, Nguyen-Q-Rieu, Deguchi S. 1990, A&A 230, 431
Walmsley CM, Churchwell E, Nash A, Fitzpatrick E. 1982, ApJ 258, L75
Wannier PG, Sahai R. 1987, ApJ 319, 367
Young K, Keene J, Phillips TG, Betz A, Boreiko R. 1996, preprint

This article was processed by the author using Springer-Verlag LaTeX A&A style file *L-AA* version 3.